

Below Referee's comments are marked by red, our responses are in black.

Uncertainties are briefly discussed in the last paragraph of Section 3. Basically, the authors refer to the uncertainty analysis by Fytterer et al (2019) which they have re-peated. This needs to be extended. Please summarize the ideas of the uncertainty analysis (based on Fytterer et al.) and state in particular which reaction steps and reaction rates are critical for the uncertainty. This extended paragraph should be moved to the end of Section 2, i.e. the uncertainties of the method should be discussed before the results are presented.

We agree with the comment. In the revised manuscript, the uncertainty analysis was extended. First of all, we added the new Table with the list of systematic uncertainties of measured data and constants and corresponding uncertainties in derived O(<sup>1</sup>D) local concentration. The corresponding paragraph was moved to the end of Section 2 and was added by a couple of sentences (see lines 63-70 in "Manuscript with marked changes" below):

«The systematic uncertainty of retrieved data is defined by uncertainties in  $VER_{2\mu m}$ , O<sub>3</sub>, T measurements, and in the rates of chemical and physical processes included in the OH( $\nu$ ) model. We reproduced the analysis presented in Fytterer et al. (2019) (see Sect. 3.4) and took into account the uncertainties of measured data and rate constants which are shown in Table 2. The third column of the Table demonstrates the uncertainties' individual impact at derived O(<sup>1</sup>D) local concentration. It can be noted that the most critical for O(<sup>1</sup>D) are the uncertainties in T, rates of reactions (2-3), Einstein coefficients for the  $\nu = 8-9$  states, and  $VER_{2\mu m}$ . The total systematic O(<sup>1</sup>D) uncertainty was obtained by calculating the root-sum-square of all individual uncertainties. It was found to vary in the range of (37-52)% depending on the pressure level. Due to averaging, the random error of data presented below is negligible.»

Validation of the O(1D) retrievals is beyond the scope of this manuscript. Nevertheless, I would like the authors to comment on perspectives towards a future validation of these SABER retrievals.

We agree with the comment. In the revised manuscript, we added a couple of sentences in the end of Sect.4 (see lines 117-123 in "Manuscript with marked changes"):

«The analysis of this impact should be carried out with the use of a global 3D chemical transport model of the mesosphere – lower thermosphere. Additionally, it may indicate measurable characteristics of this region that could indirectly confirm the results obtained in this article. In principle, direct evidences of O(<sup>1</sup>D) layer existence in nighttime mesopause can

be established by *in situ* measurements of O(<sup>1</sup>D) airglow at 630 nm which can be carried out, for example, as a part of future WADIS rocket sounding mission (Strelnikov et al., 2019; Grygalashvyly et al., 2019). More detailed analysis is out of this short article scopes.»

**Some minor comments:**

In the revised manuscript, all these points were corrected accordingly.

**Line 9, 11: remove "the" before "values" (3 times)**

Done. See lines 10 and 12 in “Manuscript with marked changes”.

**Line 13: "a useful data set"**

Done. See line 14.

**Line 14: "on the chemistry"**

Done. See line 14.

**Line 31: replace "constant" by "a continuous"**

Done. See line 15.

**Line 34: "via the process"**

Done. See line 35.

**Line 54: "use the known"**

Done. See line 56.

**Line 77: "Half a year"**

Done. See line 86.

**Line 78: "A similar pattern"**

Done. See line 87.

**Line 83: "There is a pronounced"**

Done. See line 92.

Line 84: "found similar features"

Done. See line 93.

Line 84-85: I do not understand the notation "nighttime ozone chemical equilibrium boundary", in particular the term "boundary". Please clarify.

The sentence was corrected. See lines 94-95.

Line 86: "of the stratospheric"

Done. See line 95.

Line 93: remove "the" before "values" (2 times)

Done. See line 103.

Line 94: remove the word "correspondingly"

Done. See line 104.

Line 98: replace "summarized" by "the total"

Done. See line 68.

Line 108: "use of a global"

Done. See line 118.

# Nighttime O(<sup>1</sup>D) distributions in the mesopause region derived from SABER data

Mikhail Yu. Kulikov<sup>1,2</sup>, and Mikhail V. Belikovich<sup>1</sup>

<sup>1</sup>Institute of Applied Physics of the Russian Academy of Sciences, 46 Ulyanov Str., 603950 Nizhny Novgorod, Russia

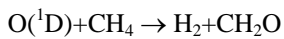
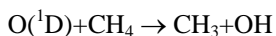
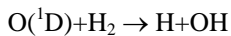
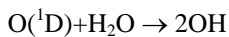
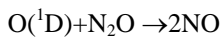
<sup>2</sup>Lobachevsky State University of Nizhni Novgorod, 23 Gagarin Avenue, 603950 Nizhny Novgorod, Russia

Correspondence to: Mikhail Yu. Kulikov (mikhail\_kulikov@mail.ru)

**Abstract.** In this study, the new source of O(<sup>1</sup>D) in the mesopause region due to the process  $\text{OH}(\nu \geq 5) + \text{O}(\text{}^3\text{P}) \rightarrow \text{OH}(0 \leq \nu' \leq \nu - 5) + \text{O}(\text{}^1\text{D})$  is applied to SABER data to estimate the nighttime O(<sup>1</sup>D) distributions for the years 2003-2005. It is found that O(<sup>1</sup>D) evolutions in these years are very similar to each other. Depending on the month, monthly averaged O(<sup>1</sup>D) distributions demonstrate from 2 to 4 maxima with ~~the~~-values up to 340 cm<sup>-3</sup> which are localized in height (at ~92-96 km) and latitude (at ~20-40°S,N and ~60-80°S,N). Annually averaged distributions in 2003-2005 have a one weak maximum at ~93 km and ~65°S with ~~the~~-values of 150-160 cm<sup>-3</sup> and 3 pronounced maxima (with ~~the~~ values up to 230 cm<sup>-3</sup>) at ~95 km and ~35°S, at ~94 km and ~40°N, at ~93 km and ~65-75°N correspondingly. In general, there is slightly more O(<sup>1</sup>D) in the northern hemisphere than in the southern hemisphere. The obtained results are a useful data set for subsequent estimation of nighttime O(<sup>1</sup>D) influence on the chemistry of the mesopause region.

## 1 Introduction

Daytime O(<sup>1</sup>D) is considered to be one of the important chemical minor species of the stratosphere, mesosphere and thermosphere, as it plays a significant role in the chemistry, and the radiative and thermal balance of this region (Brasseur & Solomon, 2005). First of all, formed by photolysis of O<sub>2</sub> and O<sub>3</sub>, O(<sup>1</sup>D) is a mediator involved in the transformation of absorbed solar radiation energy into the heating of this region and, in particular, excitation of N<sub>2</sub>( $\nu$ ) and CO<sub>2</sub>( $\nu$ ) (Harris & Adams, 1983; Panka et al., 2017). Also, O(<sup>1</sup>D) atoms participate in the reactions of destruction of long-lived greenhouse gases (Baasandorj et al., 2012), CH<sub>4</sub> oxidation, and HO<sub>x</sub> and NO<sub>x</sub> production, for example:



Moreover, the red line emission from O(<sup>1</sup>D) atoms is one of the most important airglow phenomenon which are used as a diagnostic of the ionosphere, for example, to monitor the electron density and neutral winds in the F region (Shepherd et al., 2019). Therefore, many papers and experimental campaigns are devoted to measurements of features of O<sub>3</sub> photolysis to O(<sup>1</sup>D) (Taniguchi et al., 2003; Hofzumahaus et al., 2004).

Until recently, it was believed that the above mentioned processes stop at night as ~~constant~~ continuous source of O(<sup>1</sup>D) is absent while the life time of the component is extremely low (less than 1 s). In principle, O(<sup>1</sup>D) can be generated in sprite halos but for a short duration of 1 ms (Hiraki et al., 2004). Recently, Sharma et al. (2015) and Kalogerakis et al. (2016) basing on laboratory experiments proposed that O(<sup>1</sup>D) could be produced in the mesopause region via the process  $\text{OH}(\nu \geq 5) + \text{O}(\text{}^3\text{P}) \rightarrow \text{OH}(0 \leq \nu' \leq \nu - 5) + \text{O}(\text{}^1\text{D})$ , that is multiquantum quenching of high excited states of OH by collisions with atomic oxygen in ground state.

38 Last year, Kalogerakis (2019) showed that a new model of O<sub>2</sub> A-band, that takes this process into account, describes well  
 39 (qualitatively and quantitatively) the results of early nighttime rocket measurements of volume emission rate profiles of this  
 40 airglow. Thus, he proved that the process OH( $\nu \geq 5$ ) + O(<sup>3</sup>P) → OH(0 ≤  $\nu' \leq \nu - 5$ ) + O(<sup>1</sup>D) really took place in nighttime  
 41 mesopause, and the produced O(<sup>1</sup>D) distributions can be evaluated from available data.

42 In this study, the new source of O(<sup>1</sup>D) in the mesopause region is applied to SABER data to estimate the O(<sup>1</sup>D) nighttime  
 43 distributions for the years 2003-2005.

## 44 2 O(<sup>1</sup>D) derivation from SABER Data

45 All processes used for O(<sup>1</sup>D) determination are summarized in Table 1. Here, we apply the new OH( $\nu$ ) model of Fytterer et  
 46 al. (2019). Their “best-fit model” includes all commonly used production and loss processes of OH( $\nu$ ) (see Table 1), but  
 47 some parameters of the model, in particular, branching ratios of quenching OH( $\nu$ )+O<sub>2</sub> and rate coefficients of OH( $\nu \geq 5$ ) +  
 48 O(<sup>3</sup>P) → OH(0 ≤  $\nu' \leq \nu - 5$ ) + O(<sup>1</sup>D) were adjusted with the use of volume emission rate profiles in four different wavelengths  
 49 measured by SABER and SCIAMACHY.

50 Due to low values of chemical lifetimes (less than 1 s), O(<sup>1</sup>D) can be considered in chemical equilibrium:

$$51 \quad O(^1D) = \frac{k_9 \cdot OH(9) \cdot O(^3P) + k_{10} \cdot OH(8) \cdot O(^3P) + k_{11} \cdot OH(7) \cdot O(^3P) + k_{12} \cdot OH(6) \cdot O(^3P) + k_{13} \cdot OH(5) \cdot O(^3P)}{k_{14} + k_{15} \cdot O_2 + k_{16} \cdot N_2} \quad (21)$$

52 Thus, to calculate local value of O(<sup>1</sup>D) we should specify the local concentrations of OH( $\nu=5-9$ ) and O(<sup>3</sup>P). The mentioned  
 53 model lets us to derive the OH( $\nu$ ) concentrations as the functions of the OH( $\nu$ ) source due to the reaction (1) ( $P_{OH} = k_1 \cdot H \cdot$   
 54  $O_3$ ), air concentration (M), temperature (T), and O(<sup>3</sup>P) concentration:

$$55 \quad OH(\nu) = F_\nu(P_{OH}, M, T, O(^3P)) \quad (32)$$

56 To determine O(<sup>3</sup>P) and  $P_{OH}$ , we use [the](#) known (e.g., Mlynczak et al., 2013, 2018) approach for O(<sup>3</sup>P) derivation from the  
 57 simultaneous SABER measurements of volume emission rate of (9-7) and (8-6) OH transitions ( $VER_{2\ \mu m}$ ), O<sub>3</sub> (9.6  $\mu m$ ), and  
 58 temperature (T). The approach employs the chemical equilibrium condition for nighttime ozone. As the result, it is done with  
 59 the use of the following system of equations:

$$60 \quad \begin{cases} P_{OH} = k_2 \cdot O(^3P) \cdot O_2 \cdot M - k_3 \cdot O(^3P) \cdot O_3 \\ VER_{2\ \mu m} = k_4(9,7) \cdot F_9(P_{OH}, M, T, O(^3P)) + k_4(8,6) \cdot F_8(P_{OH}, M, T, O(^3P)) \end{cases} \quad (43)$$

61 Thus, we derive the local values of O(<sup>3</sup>P),  $P_{OH}$ , and OH( $\nu=5-9$ ) from SABER data with the use of eqs. (2-3-4) and apply sets  
 62 of data (T, M, OH( $\nu=5-9$ ), and O(<sup>3</sup>P)) to retrieve the local concentrations of O(<sup>1</sup>D) with the use of eq. (21).

63 The systematic uncertainty of retrieved data is defined by uncertainties in  $VER_{2\ \mu m}$ , O<sub>3</sub>, T measurements, and in the rates of  
 64 chemical and physical processes included in the OH( $\nu$ ) model. We reproduced the analysis presented in Fytterer et al. (2019)  
 65 (see Sect. 3.4) and took into account the uncertainties of measured data and rate constants which are shown in Table 2. The  
 66 third column of the Table demonstrates the uncertainties' individual impact at derived O(<sup>1</sup>D) local concentration. It can be  
 67 noted that the most critical for O(<sup>1</sup>D) are the uncertainties in T, rates of reactions (2-3), Einstein coefficients for the  $\nu = 8-9$   
 68 states, and  $VER_{2\ \mu m}$ . The total systematic O(<sup>1</sup>D) uncertainty was obtained by calculating the root-sum-square of all  
 69 individual uncertainties. It was found to vary in the range of (37-52)% depending on the pressure level. Due to averaging, the  
 70 random error of data presented below is negligible.

## 71 3 O(<sup>1</sup>D) nighttime distributions

72 We use the version 2.0 of the SABER data product (Level2A) for the simultaneously measured  $VER_{2\ \mu m}$ , O<sub>3</sub>, and T profiles  
 73 within the 0.01–0.0001 hPa pressure ( $p$ ) interval (approximately 80–105 km in 2003-2005. We take only nighttime data  
 74 when the solar zenith angle  $\chi > 95^\circ$ . The range of latitudes covered by the satellite trajectory in a month was divided into 20  
 75 bins  $\sim (5.5-8)^\circ$  each. 1500-3000 single profiles of O(<sup>1</sup>D) concentration fall into one bin during a month of SABER

76 observations. For each bin we calculate monthly averaged zonal mean  $\langle O(^1D) \rangle$  distributions (hereafter, the angle brackets  
77 are used to denote timely and spatially averaged values). For annually averaged distributions, we use 40 bins  $\sim 4^\circ$  each.  
78 Monthly averaged  $\langle O(^1D) \rangle$  distributions in corresponding month of 2003-2005 are shown in Figs. 1–3. Let's analyze the  
79 presented data using the distributions in 2003 as an example. Depending on the range of latitudes covered by the satellite  
80 trajectory in specified month, the figures show from 2 to 4 maxima which are localized in height (at  $\sim 92$ - $96$  km) and latitude  
81 (at  $\sim 20$ - $40^\circ$ S,N and  $\sim 60$ - $80^\circ$ S,N). The values of the maxima can reach up to  $300 \text{ cm}^{-3}$  and more in both hemispheres and  
82 different months, for example, in January-March and in May-August. Nevertheless, annual cycle of southern  $O(^1D)$   
83 demonstrates certain differences from northern one, i.e. many features of  $\langle O(^1D) \rangle$  in the southern hemisphere are not  
84 repeated in the northern hemisphere with a shift of 6 months. In particular, the distributions in January-February show 2  
85 pronounced maxima with close values (up to  $300 \text{ cm}^{-3}$ ): the first one is at  $\sim 95$  km and  $\sim 50$ - $60^\circ$ S, the second one is at  $\sim 93$  km  
86 and  $\sim 60$ - $80^\circ$ N. Half a year later (in July-August), we can see 1-2 weak maxima in the southern hemisphere and a strongly  
87 pronounced maximum at  $\sim 95$  km and  $\sim 40$ - $50^\circ$ N. ~~The~~ similar pattern can be noticed comparing the  $\langle O(^1D) \rangle$   
88 distributions in June and December. The satellite trajectory in March and September allows us to observe simultaneously 4  
89 maxima. Note that the southern high-latitudinal maximum (up to  $340 \text{ cm}^{-3}$ ) in March does not correspond to the relatively  
90 weak northern high- latitudinal maximum in September.

91 The  $\langle O(^1D) \rangle$  evolutions in 2004-2005 are very similar to 2003. Nevertheless, one can see some differences. First of all, in  
92 January-February 2004, there is a pronounced particularity above  $60^\circ$ N below 90 km which does not appear in 2003 and  
93 2005. Kulikov et al. (2019) found ~~the~~ similar features in the latitude dependence of nighttime ozone chemical equilibrium  
94 boundary (the lower boundary of the altitudinal-latitudinal region where this equilibrium is satisfied (Belikovich et al., 2018;  
95 Kulikov et al., 2018)) in January–March 2004 above  $60^\circ$ N and connected it with abnormal dynamics of the stratospheric  
96 polar vortex during 2003–2004 Arctic winter. There are additional features also which take place in a specific year, but  
97 absent in other two years. In particular, the northern high-latitudinal maximum in January-February 2003 is remarkably  
98 higher (by the value) than the ones in January-February 2004-2005. The southern high-latitudinal maximum (up to  $340 \text{ cm}^{-3}$ )  
99 in March 2003 corresponds to the same maximum in March 2005 but both maxima are remarkably higher than the one in  
100 March 2004. The reverse (relative to December 2003 and 2005) ratio can be observed for the values of southern and northern  
101 maxima in December 2004.

102 Annually averaged  $\langle O(^1D) \rangle$  distributions in 2003-2005 are shown in Fig. 4. There can be seen one weak maximum at  
103  $\sim 93$  km and  $\sim 65^\circ$ S with ~~the~~ values of  $150$ - $160 \text{ cm}^{-3}$  and 3 pronounced maxima (with ~~the~~ values up to  $230 \text{ cm}^{-3}$ ) at  $\sim 95$  km  
104 and  $\sim 35^\circ$ S, at  $\sim 94$  km and  $\sim 40^\circ$ N, at  $\sim 93$  km and  $\sim 65$ - $75^\circ$ N ~~correspondingly~~. In general, there is slightly more  $O(^1D)$  in the  
105 northern hemisphere than in the southern hemisphere.

~~The systematic uncertainty of presented data is defined mainly by uncertainties in  $VER_{2\text{-}\mu\text{m}}$ ,  $O_3$ , T measurements, and in the  
107 rates of chemical and physical processes included in the OH( $\nu$ ) model. We repeated the analysis presented in Fyterer et al.  
108 (2019) (see Sect. 3.4) and found that summarized uncertainty of  $O(^1D)$  varied in the range of (37-52)% depending on the  
109 pressure level. Due to averaging, the random error of presented data is negligible.~~

#### 111 4 Discussion and Conclusion

112 According to various early papers (Nicolet, 1959; Ghosh & Gupta, 1970; Shimazaki & Laird, 1970; Harris & Adams, 1983),  
113 daytime  $O(^1D)$  concentrations at 90-100 km varied in the range of  $(10^2$ - $10^3) \text{ cm}^{-3}$ . Brasseur & Solomon (2005) published the  
114 table (see Table A.6.2.c) where daytime  $O(^1D)$  changed from  $70 \text{ cm}^{-3}$  at 90 km to  $140 \text{ cm}^{-3}$  at 100 km. The presented results  
115 show that monthly and annually mean nighttime  $O(^1D)$  concentrations at these altitudes can reach  $300 \text{ cm}^{-3}$  and  $200 \text{ cm}^{-3}$ ,  
116 respectively. Thus, nighttime concentrations of  $O(^1D)$  are comparable with daytime concentrations of this component and, in

117 principle, can impact noticeably the chemistry and thermal balance of the mesopause region. ~~More detailed~~The analysis of  
118 this impact should be carried out with the use of ~~the~~ global 3D chemical transport model of the mesosphere – lower  
119 thermosphere. Additionally, it may indicate measurable characteristics of this region that could indirectly confirm the results  
120 obtained in this article. In principle, direct evidences of O(<sup>1</sup>D) layer existence in nighttime mesopause can be established by  
121 in situ measurements of O(<sup>1</sup>D) airglow at 630 nm which can be carried out, for example, as a part of future WADIS rocket  
122 sounding mission (Strelnikov et al., 2019; Grygalashvyly et al., 2019). More detailed analysis is out of this short article  
123 scopes.

124 **Data availability.** The SABER data used in this study can be downloaded from ftp://saber.gats-  
125 inc.com/Version2\_0/Level2A/. The presented data can be downloaded from  
126 http://www.iapras.ru/english/structure/dep\_240/dep\_240.html.

127 **Author contributions.** Both authors contributed equally to this paper.

128 **Competing interests.** The authors declare that they have no conflict of interest.

129 **Acknowledgments.** The work was carried out at the expense of the state assignment #0729-2020-0037. The authors are  
130 grateful to the SABER team for data availability.

## 131 References

132 Adler-Golden, S.: Kinetic parameters for OH nightglow modeling consistent with recent laboratory measurements, J.  
133 Geophys. Res., 102, 19969–19976, doi:10.1029/97JA01622, 1997.

134 Baasandorj, M., Hall, B. D., and Burkholder, J. B.: Rate coefficients for the reaction of O(<sup>1</sup>D) with the atmospherically long-  
135 lived greenhouse gases NF<sub>3</sub>, SF<sub>5</sub>CF<sub>3</sub>, CHF<sub>3</sub>, C<sub>2</sub>F<sub>6</sub>, c-C<sub>4</sub>F<sub>8</sub>, n-C<sub>5</sub>F<sub>12</sub>, and n-C<sub>6</sub>F<sub>14</sub>. Atmos. Chem. Phys., 12, 11753–11764,  
136 doi:10.5194/acp-12-11753-2012, 2012.

137 Belikovich, M. V., Kulikov, M. Y., Grygalashvyly, M., Sonnemann, G. R., Ermakova, T. S., Nechaev, A. A., and Feigin, A.  
138 M.: Ozone chemical equilibrium in the extended mesopause under the nighttime conditions, Adv. Sp. Res., 61(1), 426–432,  
139 doi:10.1016/j.asr.2017.10.010, 2018.

140 Brasseur, G. P., and Solomon, S.: Aeronomy of the middle atmosphere: Chemistry and physics of the stratosphere and  
141 mesosphere (3rd ed). Dordrecht, Netherlands: Springer Science and Business Media, 2005.

142 Burkholder, J. B., Sander, S. P., Abbatt, J., Barker, J. R., Huie, R. E., Kolb, C. E., et al.: Chemical kinetics and  
143 photochemical data for use in atmospheric studies, evaluation no. 18, JPL Publication 15–10, Pasadena, CA: Jet Propulsion  
144 Laboratory, http://jpldataeval.jpl.nasa.gov, 2015.

145 Caridade, P. J. S. B., Horta, J.-Z. J., and Varandas, A. J. C.: Implications of the OCOH reaction in hydroxyl nightglow  
146 modeling, Atmos. Chem. Phys., 13, 1–13, doi:10.5194/acp-13-1-2013, 2013.

147 Fytterer, T., von Savigny, C., Mlynczak, M., and Sinnhuber, M.: Model results of OH airglow considering four different  
148 wavelength regions to derive night-time atomic oxygen and atomic hydrogen in the mesopause region, Atmos. Chem. Phys.,  
149 19, 1835–1851, doi:10.5194/acp-19-1835-2019, 2019.

150 García-Comas, M., López-Puertas, M., Marshall, B. T., Wintersteiner, P. P., Funke, B., Bermejo-Pantaleón, D., Mertens,



151 [C. J., Remsberg, E. E., Gordley, L. L., Mlynczak, M. G., and Russell III, J. M.: Errors in Sounding of the Atmosphere using](#)  
152 [Broadband Emission Radiometry \(SABER\) kinetic temperature caused by non-local-thermodynamic equilibrium model](#)  
153 [parameters. J. Geophys. Res., 113, D24106, doi:10.1029/2008JD010105, 2008.](#)

154 Ghosh, S. N., and Gupta, S. K.: Altitude distributions of and radiations from certain oxygen and nitrogen metastable  
155 constituents, J. Geomagn. Geoelectr., 22, 329-339, 1970.

156 [Grygalashvyly, M., Eberhart, M., Hedin, J., Strelnikov, B., Lübken, F.-J., Rapp, M., Löhle, S., Fasoulas, S., Khaplanov, M.,](#)  
157 [Gumbel, J., and Vorobeva, E.: Atmospheric band fitting coefficients derived from a self-consistent rocket-borne experiment,](#)  
158 [Atmos. Chem. Phys., 19, 1207–1220, doi:10.5194/acp-19-1207-2019, 2019.](#)

159 Harris, R. D., and Adams, G. W.: Where does the O(<sup>1</sup>D) energy go? J. Geophys. Res., 88(A6), 4918–4928,  
160 doi:10.1029/JA088iA06p04918, 1983.

161 Hiraki, Y., Tong, L., Fukunishi, H., Nanbu, K., Kasai, Y., and Ichimura, A.: Generation of metastable oxygen atom O(<sup>1</sup>D) in  
162 sprite halos, Geophys. Res. Lett., 31, L14105, doi:10.1029/2004GL020048, 2004.

163 Hofzumahaus, A., Lefer, B. L., Monks, P. S., Hall, S. R., Kylling, A., Mayer B. et al.: Photolysis frequency of O<sub>3</sub> to O(<sup>1</sup>D):  
164 Measurements and modeling during the International Photolysis Frequency Measurement and Modeling Intercomparison  
165 (IPMMI), J. Geophys. Res., 109, D08S90, doi:10.1029/2003JD004333, 2004.

166 Hunt, B. G.: A diffusive-photochemical study of the mesosphere and lower thermosphere and the associated conservation  
167 mechanisms, J. Atm. Terr. Phys., 33, 1869-1892, 1971.

168 Kalogerakis, K. S., Smith, G. P., and Copeland, R. A.: Collisional removal of OH(X <sup>2</sup>Π, v = 9) by O, O<sub>2</sub>, O<sub>3</sub>, N<sub>2</sub>, and CO<sub>2</sub>. J.  
169 Geophys. Res., 116, D20307, doi:10.1029/2011JD015734, 2011.

170 Kalogerakis, K. S., Matsiev, D., Sharma, R. D., and Wintersteiner, P. P.: Resolving the mesospheric nighttime 4.3 μm  
171 emission puzzle: Laboratory demonstration of new mechanism for OH(v) relaxation, Geophys. Res. Lett., 43, 8835–8843,  
172 doi:10.1002/2016GL069645, 2016.

173 Kalogerakis, K. S.: A previously unrecognized source of the O<sub>2</sub> atmospheric band emission in earth's nightglow. Science  
174 Advances, 5, eaau9255, doi:10.1126/sciadv.aau9255, 2019.

175 Kulikov, M. Y., Belikovich, M. V., Grygalashvyly, M., Sonnemann, G. R., Ermakova, T. S., Nechaev, A. A., and Feigin, A.  
176 M.: Nighttime ozone chemical equilibrium in the mesopause region, J. Geophys. Res., 123, 3228–3242,  
177 doi:10.1002/2017JD026717, 2018.

178 Kulikov, M. Yu., Nechaev, A. A., Belikovich, M. V., Vorobeva, E. V., Grygalashvyly, M., Sonnemann, G. R., and Feigin,  
179 A. M.; Border of nighttime ozone chemical equilibrium in the mesopause region from saber data: implications for derivation  
180 of atomic oxygen and atomic hydrogen, Geophys. Res. Lett., 46, 997–1004, doi:10.1029/2018GL080364, 2019.

181 Mlynczak, M. G., Hunt, L. A., Mast, J. C., Marshall, B. T., Russell III, J. M., Smith, A. K., Siskind, D. E., Yee, J.-H.,  
182 Mertens, C. J., Martin-Torres, F. J., Thompson, R. E., Drob, D. P., and Gordley, L. L.: Atomic oxygen in the mesosphere and  
183 lower thermosphere derived from SABER: Algorithm theoretical basis and measurement uncertainty, J. Geophys. Res., 118,  
184 5724–5735, doi:10.1002/jgrd.50401, 2013.

185 Mlynczak, M. G., Hunt, L. A., Russell, J. M., III, and Marshall, B. T.: Updated SABER night atomic oxygen and  
186 implications for SABER ozone and atomic hydrogen, Geophys. Res. Lett., 45, 5735–5741, doi:10.1029/2018GL077377,  
187 2018.

188 Nicolet, M.: The constitution and composition of the upper atmosphere, Proc. IRE, 47, 142-147, 1959.

189 Panka, P. A., Kutepov, A. A., Kalogerakis, K. S., Janches, D., Russell, J. M., Rezac, L., Feofilov, A. G., Mlynczak, M. G.,  
190 and Yiğit, E.: Resolving the mesospheric nighttime 4.3 μm emission puzzle: Comparison of the CO<sub>2</sub>(ν<sub>3</sub>) and OH(v)  
191 emission models, Atm. Chem. Phys., 17, 9751–9760, doi:10.5194/acp-17-9751-2017, 2017.



192 Sharma, R. D., Wintersteiner, P. P., and Kalogerakis, K. S.: A new mechanism for OH vibrational relaxation leading to  
193 enhanced CO<sub>2</sub> emissions in the nocturnal mesosphere, *Geophys. Res. Lett.*, 42, 4639–4647, doi:10.1002/2015GL063724,  
194 2015.

195 Shepherd, M., Shepherd, G., and Codrescu, M.: Perturbations of O(<sup>1</sup>D) VER, temperature, winds, atomic oxygen, and TEC  
196 at high southern latitudes, *J. Geophys. Res.*, 124, 4773–4795, doi:10.1029/2019JA026480, 2019.

197 Shimazaki, T., and Laird, A. R.: A model calculation of the diurnal variation in minor neutral constituents in the mesosphere  
198 and lower thermosphere including transport effects, *J. Geophys. Res.*, 75, 3221– 3235, doi:10.1029/JA075i016p03221, 1970.

199 [Strelnikov, B., Eberhart, M., Friedrich, M., Hedin, J., Khaplanov, M., Baumgarten, G., Williams, B. P., Staszak, T., Asmus,  
200 H., Strelnikova, I., Latteck, R., Grygalashvyly, M., Lübken, F.-J., Höffner, J., Wörl, R., Gumbel, J., Löhle, S., Fasoulas, S.,  
201 Rapp, M., Barjatya, A., Taylor, M. J., and Pautet, P.-D.: Simultaneous in situ measurements of small-scale structures in  
202 neutral, plasma, and atomic oxygen densities during the WADIS sounding rocket project, \*Atmos. Chem. Phys.\*, 19, 11443–  
203 11460, <https://doi.org/10.5194/acp-19-11443-2019>, 2019.](#)

204 Taniguchi, N., Hayashida, S., Takahashi, K., and Matsumi, Y.: Sensitivity studies of the recent new data on O(<sup>1</sup>D) quantum  
205 yields in O<sub>3</sub> Hartley band photolysis in the stratosphere, *Atmos. Chem. Phys.*, 3, 1293-1300, doi:10.5194/acp-3-1293-2003,  
206 2003.

207 Varandas, A. J. C.: Reactive and non-reactive vibrational quenching in OCOH collisions, *Chem. Phys. Lett.*, 396, 182–190,  
208 doi:10.1016/j.cplett.2004.08.023, 2004.

209 Xu, J., Gao, H., Smith, A. K., and Zhu, Y.: Using TIMED/SABER nightglow observations to investigate hydroxyl emission  
210 mechanisms in the mesopause region, *J. Geophys. Res.*, 117, D02301, doi:10.1029/2011JD016342, 2012.

211

212 **Table 1. List of processes.**

213

|    | Process  | Rate  | Reference  |
|----|--|---|--|
| 1  | $\text{H} + \text{O}_3 \rightarrow \text{O}_2 + \text{OH}(v)$                              | $k_{\text{T}}, k_{\text{T}(+)}, k_1$<br>$k_1(v) = k_1 \cdot f(v)$ | Burkholder et al. (2015) <sup>7</sup> ,<br>Alder-Golden (1997, Table 1)              |
| 2  | $\text{O}(^3\text{P}) + \text{O}_2 + \text{M} \rightarrow \text{O}_3 + \text{M}$           | $k_2$   | Burkholder et al. (2015)   |
| 3  | $\text{O}(^3\text{P}) + \text{O}_3 \rightarrow 2\text{O}_2$                                | $k_3$   | Burkholder et al. (2015)   |
| 4  | $\text{OH}(v) \rightarrow \text{OH}(v') + h\nu$  | $k_4(v, v')$  | Xu et al. (2012, Table A1)   |
| 5  | $\text{OH}(v) + \text{N}_2 \rightarrow \text{OH}(v') + \text{N}_2$                         | $k_5(v, v')$  | Alder-Golden (1997, Table 1),<br>Kalogerakis et al. (2011)                           |
| 6  | $\text{OH}(v) + \text{O}_2 \rightarrow \text{OH}(v') + \text{O}_2$                         | $k_6(v, v')$  | Alder-Golden (1997, Table 3),<br>corrected and adjusted by Fytterer<br>et al. (2019) |
| 7  | $\text{OH}(v) + \text{O}(^3\text{P}) \rightarrow \text{H} + \text{O}_2$                    | $k_7(v)$  | Varandas (2004, Table 3, M I)  |
| 8  | $\text{OH}(v) + \text{O}(^3\text{P}) \rightarrow \text{OH}(v') + \text{O}$                 | $k_8(v, v')$  | Caridade et al. (2013, Table 1)  |
| 9  | $\text{OH}(9) + \text{O}(^3\text{P}) \rightarrow \text{OH}(3,4) + \text{O}(^1\text{D})$    | $k_9$   | Fytterer et al. (2019)   |
| 10 | $\text{OH}(8) + \text{O}(^3\text{P}) \rightarrow \text{OH}(3) + \text{O}(^1\text{D})$      | $k_{10}$  | Fytterer et al. (2019)   |
| 11 | $\text{OH}(7) + \text{O}(^3\text{P}) \rightarrow \text{OH}(\leq 2) + \text{O}(^1\text{D})$ | $k_{11}$  | Fytterer et al. (2019)   |
| 12 | $\text{OH}(6) + \text{O}(^3\text{P}) \rightarrow \text{OH}(\leq 1) + \text{O}(^1\text{D})$ | $k_{12}$  | Fytterer et al. (2019)   |
| 13 | $\text{OH}(5) + \text{O}(^3\text{P}) \rightarrow \text{OH} + \text{O}(^1\text{D})$         | $k_{13}$  | Fytterer et al. (2019)   |
| 14 | radiative decay of $\text{O}(^1\text{D})$  | $k_{14}$  | Burkholder et al. (2015)   |
| 15 | $\text{O}(^1\text{D}) + \text{O}_2 \rightarrow \text{O}(^3\text{P}) + \text{O}_2$          | $k_{15}$  | Burkholder et al. (2015)   |
| 16 | $\text{O}(^1\text{D}) + \text{N}_2 \rightarrow \text{O} + \text{N}_2$                      | $k_{16}$  | Burkholder et al. (2015)   |

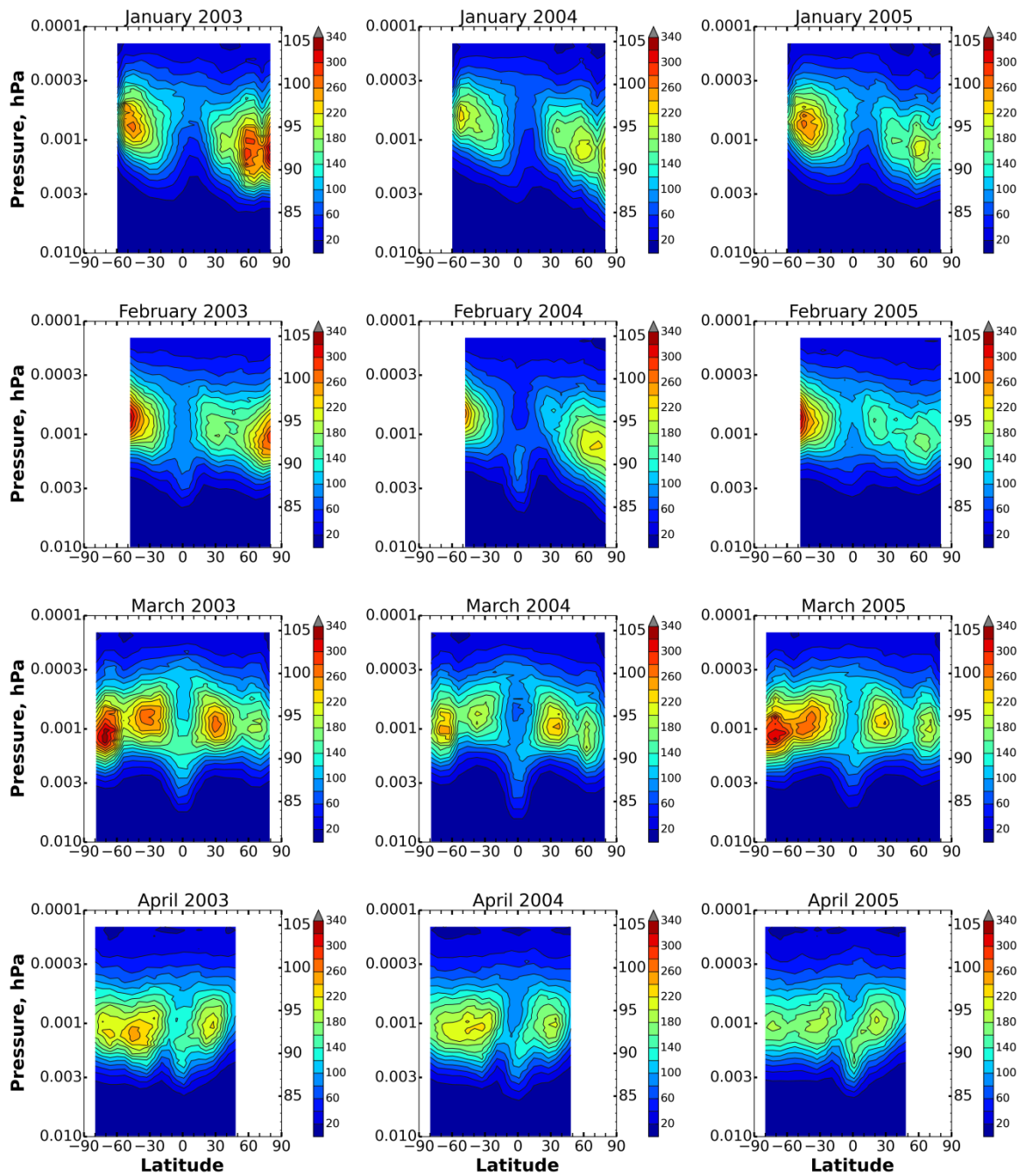
214

215 **Table 2. List of systematic uncertainties of measured data and rate constants and corresponding uncertainties in**  
 216 **derived  $\text{O}(^1\text{D})$  local concentration.**

| <u>Measured characteristic<br/>or rate</u> | <u>Its uncertainty</u>          | <u><math>\text{O}(^1\text{D})</math> uncertainty, %</u> |
|--|---------------------------------|---|
| $VER_{2\ \mu\text{m}}$                     | 6%                              | 11-17.5   |
| $\text{O}_3$                               | 10%                             | 0.1-8.2   |
| $\text{I}$                                 | from García-Comas et al. (2008) | 0.1-29.7  |
| $k_2$                                      | from Burkholder et al. (2015)   | 14-30.5   |
| $k_3$                                      | from Burkholder et al. (2015)   | 0.7-19.5  |
| $k_{15}$                                   | from Burkholder et al. (2015)   | 2.6-2.8   |
| $k_{16}$                                   | from Burkholder et al. (2015)   | 8-10  |
| $f(9)$                                     | 0.03                            | 1-6   |
| $f(8)$                                     | 0.03                            | 1.4-8   |
| $k_4(9, v')$                               | 30%                             | 12-23.1   |
| $k_4(8, v')$                               | 30%                             | 11-24.6   |
| $k_4(7, v')$                               | 30%                             | 0.6-1.3   |
| $k_4(6, v')$                               | 30%                             | 0.6-1.3   |
| $k_4(5, v')$                               | 30%                             | 0.3-0.9   |

217

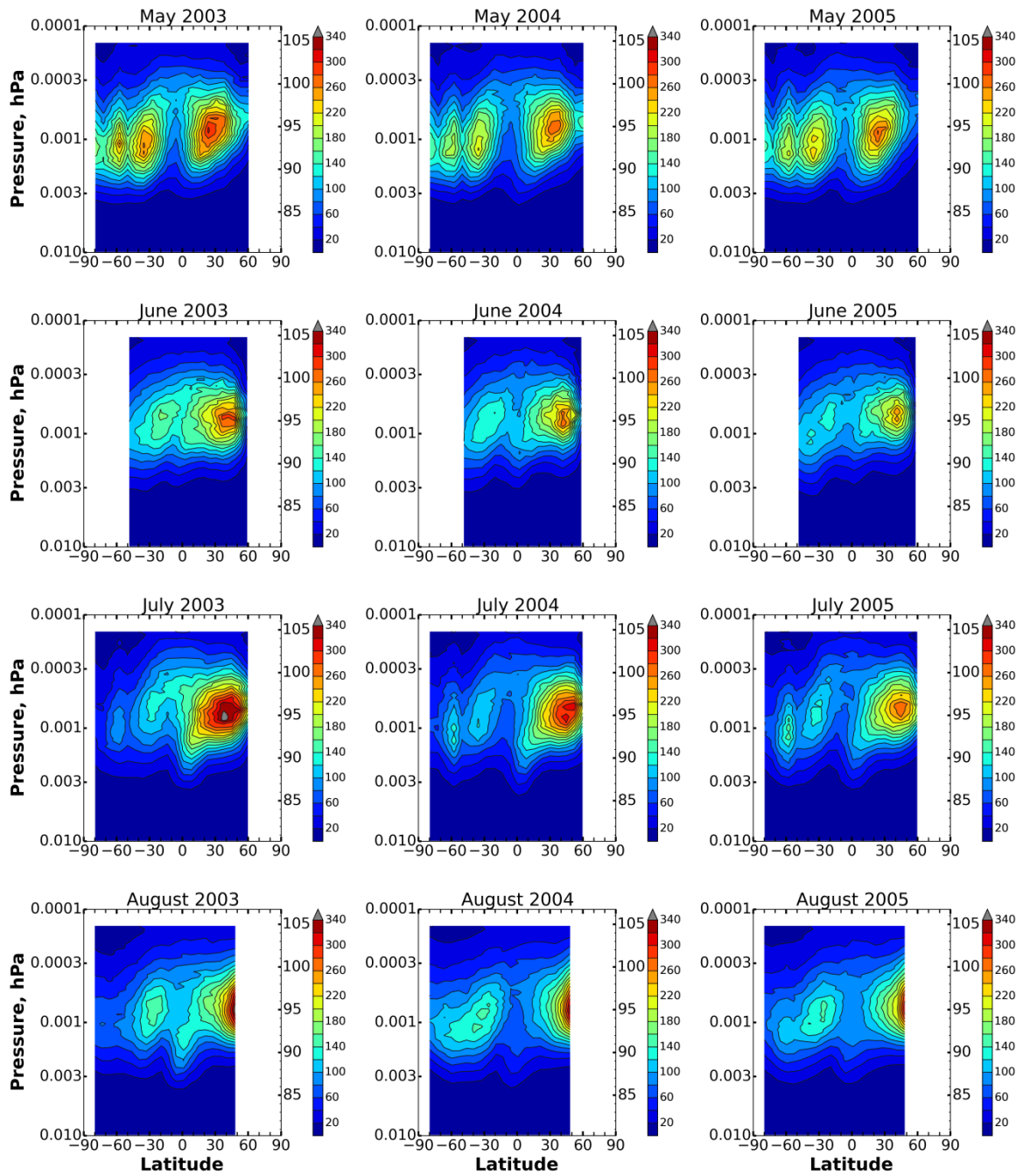
218



223 **Figure 1. Monthly averaged  $\text{O}(^1\text{D})$  concentration (in  $\text{cm}^{-3}$ ) in January-April of 2003-2005.**

225

226



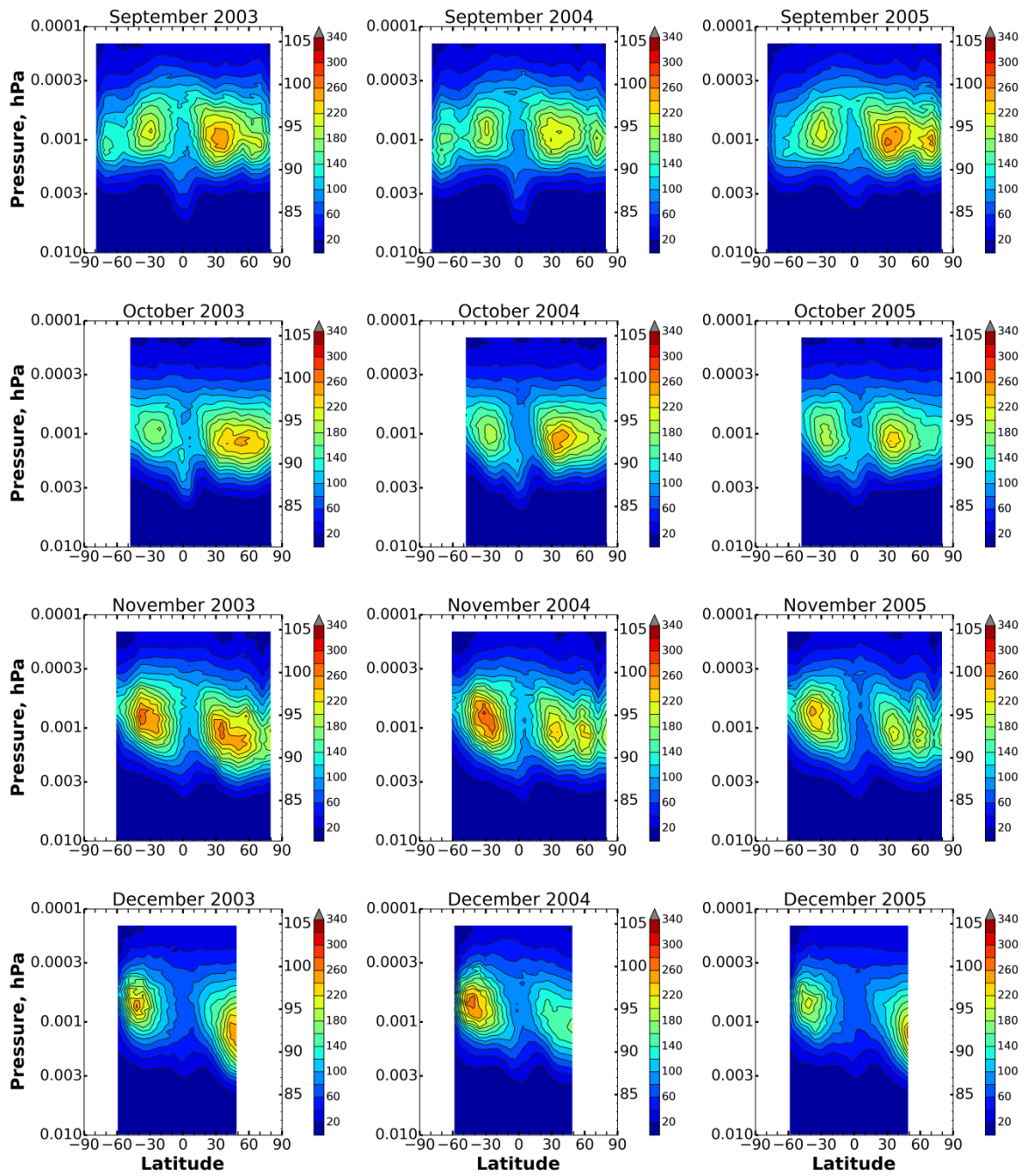
227

228 **Figure 2. Monthly averaged O(<sup>1</sup>D) concentration (in cm<sup>-3</sup>) in May-August of 2003-2005.**

229

230

231

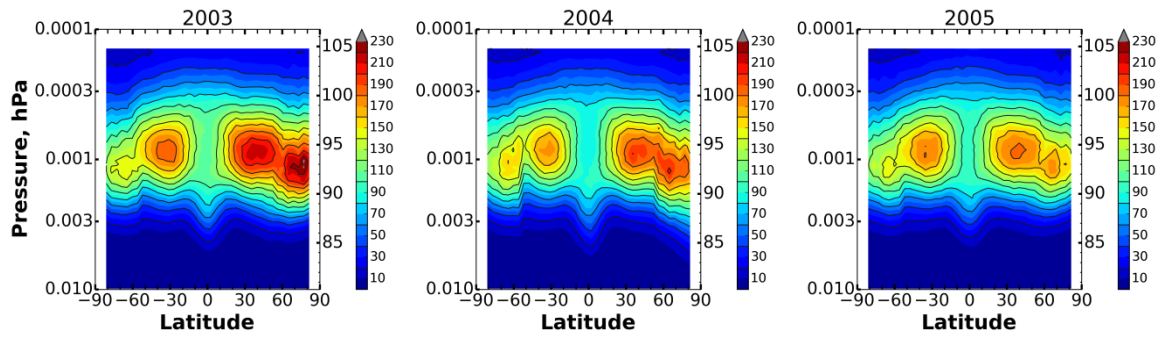


232

233 **Figure 3. Monthly averaged O(<sup>1</sup>D) concentration (in cm<sup>-3</sup>) in September-December of 2003-2005.**

234

235



236

237 **Figure 4.** Annually averaged O(<sup>1</sup>D) concentration (in cm<sup>-3</sup>) in 2003-2005.